# CrystEngComm

Accepted Manuscript






ROYAL SOCIETY OF CHEMISTRY

www.rsc.org/crystengcomm

CrystEngComm

RSCPublishing

ARTICLE

# Solid-State Investigation on a New Dimorphic Substituted *N*-Salicylidene Compound: Insights into Thermochromic Behaviour

A. Carletta[a], J. Dubois[a], A. Tilborg[a] and J. Wouters[a*]

DOI:

Received,
Accepted

DOI:

www.rsc.org/

Substituted *N*-salicylidene aniline has been quantitatively prepared by mechanochemical synthesis starting from the corresponding aniline and *ortho*-vanillin. X-ray diffraction reveals that the compound crystallizes into two different polymorphic forms, due to its conformational flexibility. *Ab initio* conformational calculations combined with CSD survey allow proper definition of the conformational space and selection of specific starting geometries for crystal structure prediction studies. Therefore, theoretical packing simulation was able to retrieve the two polymorphic structures in agreement with the experimental data. DSC calorimetric analysis provides extra information on the thermodynamic relationship between polymorphs I and II, and their exposition to liquid nitrogen, coupled with low-temperature X-ray analysis, highlights structural reasons for the intrinsic thermochromic behaviour of the compound.

## Introduction

Solid-state polymorphism in small molecules can affect various physical (shape, color, solubility or mechanical strength) and chemical (*e.g.* photochemical reactivity in the solid state) properties.[1] Moreover, for compounds presenting therapeutic properties such as API leads, polymorphism can tremendously influence their pharmaceutical outcomes.[1] Polymorphism can occur as a consequence of several different causes, but when it results from the existence of different potential conformers for the same molecule, it is generally called conformational polymorphism.[1] In the case of pharmaceutical molecules, but also for other compounds whose interest is also based on solid-state crystalline stability, isolation and characterization of different polymorphs, as well as other crystal forms (solvates, salts and co-crystals) represent an appealing area of modern solid state chemistry.[1] Therefore, significant research efforts are oriented nowadays towards the development of crystal structure prediction (CSP) methodologies aiming to identify possible polymorphic forms.[1]

In this context, we present here a solid-state structural study of *(E)-2-methoxy-6-{[(3-nitrophenyl)imino]methyl}phenol*(Compound (**1**), IUPAC systematic name, $C_{14}H_{12}N_2O_4$, Fig. 1). This kind of substituted salicylidene aniline, derived from *ortho*-hydroxybenzaldehyde (*ortho*-vanillin), can exhibit solid-state photochromism and thermochromism.[2-6] Photo- and thermochromic materials can lead to a broad range of applications, *i.e.* in information storage and electronic display systems, in optical switching devices like ophthalmic glasses or in photomechanical materials.[7-10] The compound in our study was mechanochemically synthetized by grinding of the corresponding aniline and *ortho*-vanillin. Crystallization of the ground product, by slow evaporation from different saturated solutions, led to two polymorphic forms, labelled polymorph I (orthorhombic, Pbca) and II (triclinic, $P\bar{1}$). In the two corresponding crystal structures, the compound adopts two different conformations differing by the C7-N1-C4-C3 torsion angle (T1) value. The energy barrier associated with the rotation of T1, as well as of another torsion angle of the molecule (T2), has been calculated by 1D conformational scan. The variation of the conformational energy over the values of T1 and T2 has been compared to the frequency of occurrence of related structures reported in the CSD. These data give access to the conformational space of the molecule and provide starting geometries for crystal structure prediction. Intrinsic thermochromic behaviour of the compound has also been investigated by low-temperature single crystal X-ray diffraction (SCXRD) which leads to insights into structural changes inducing this phenomenon.

## Results and discussion

Mechanochemical synthesis of (**1**), a hydroxy-substituted Schiff base,[11] has been implemented by dry ball-milling of equimolar physical mixtures of 3-nitroaniline and *ortho*-vanillin (Scheme 1). NMR and powder XRD data indicate a near-total conversion of the reactants[†] (Fig. S1, with exclusive phase formation of polymorph II) and SCXRD analysis

confirms formation of the product. Liquid-assisted grinding has also been performed with several solvents (MeOH, EtOH, 2-propOH).The phase obtained always corresponds to Form II, suggesting relative stability of this crystalline phase (see further). To obtain single crystals suitable for SCXRD, the following conditions have been applied:

*Polymorph I.* Crystals have been obtained by evaporation from a saturated solution in EtOH/MeOH (in the same proportions). Orange needle-like crystals suitable for X-ray diffraction have been obtained after 5 days.

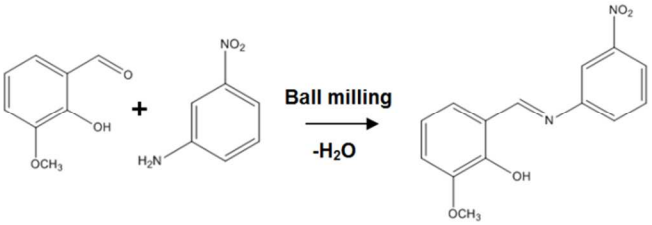


**Scheme 1** Mechanosynthesis of compound (**1**) obtained by grinding *ortho*-vanillin and 3-nitroaniline.

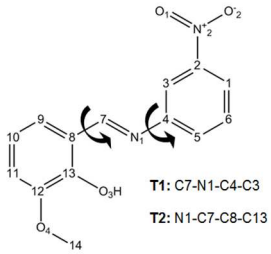


**Fig. 1** Molecular connectivity diagram and numbering scheme for compound (**1**) (*(E)-2-methoxy-6-{[(3-nitrophenyl)imino]methyl}phenol*).

*Polymorph II.* Crystals have been obtained from a saturated solution in EtOH and toluene. Red plate crystals suitable for X-ray diffraction have been obtained after 4 days.

Using crystal seeding, it is possible to obtain batches of pure polymorphs I or II from slow evaporation of concentrated solutions in EtOH/EtOAc and EtOH/acetic acid.

## Structure Determination

Single crystal X-ray diffraction analysis was performed on crystals obtained from recrystallization of saturated solutions of (**1**). Data have been collected at room temperature on both polymorphs and main crystallographic data are reported in Table 1. An extra data set has been collected at low temperature (105 K) on crystals of form I (Table T1, see further for discussion on the data). SCXRD analysis reveals that (**1**) exhibits conformational polymorphism. A coplanar conformation (T1= 1.4(2)° and T2=-0.9(2)°) is found for molecules in polymorph I whereas a 27°-tilted conformation is present in polymorph II (T1=-26.9(2)° and T2=-1.4(2)°). Therefore, molecules essentially differ for T2 torsion angle value. ORTEP diagrams are given in Figure 2. The experimental T1 value is close to 0° for both forms, allowing optimal electronic delocalization between the phenyl and iminic group.

*Polymorph I.* Crystals obtained belong to the orthorhombic Pbca space group. General organization of the crystalline network consists of π-π stacked layers crossing each other with a 53.7° angle (Fig. 3, left). As the molecule is essentially flat, an intramolecular hydrogen bond is observed in the structure, involving the hydroxyl moiety and the iminic group (Table 2). The coplanar conformation further allows existence of two different O…H short contact interactions between the nitro moiety and the hydrogen atom on C3 (N=O1…H-C3), on one side, and between the same nitro group and the hydrogen atom on the iminic carbon (N=O1…H-C7) on the other side (Fig. 3, right). π-π stacking between molecular entities arises principally following crystallographic axis [001] (Fig. 3, right), with a centroid-centroid distance of 3.63 Å (Fig. S2, Table 3).

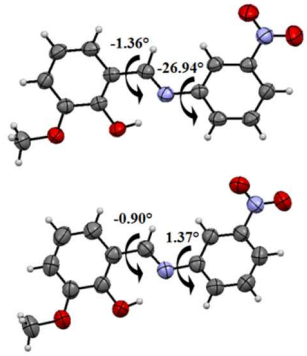


**Fig. 2** ORTEP diagram (50% probability ellipsoids) for compound (**1**) in crystals belonging to polymorph I (top) and polymorph II (bottom).

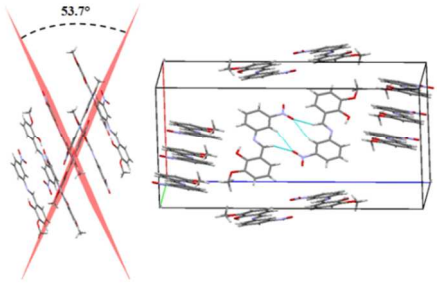


**Fig. 3** Crystal packing for Form I with intercrossing layers in the crystalline network (left) and polymorph I unit cell, with molecules forming dimers stabilized by double O···H short contact interactions (right) (distance O1-H3: 2.68(6) Å, O1-H7: 2.51(5) Å).

*Polymorph II.* Crystals obtained belong to the triclinic $P\bar{1}$ space group. General organization of the crystalline network consists of stacked layers formed by dimers. An intramolecular hydrogen bond between the hydroxyl moiety and the iminic group is detected, principally caused by a T2 value of about 0°. Molecules interact by a single O···H short contact involving the O-atom of the nitro group and the hydrogen on the iminic carbon (N=O1···H-C7) (Fig. 4).

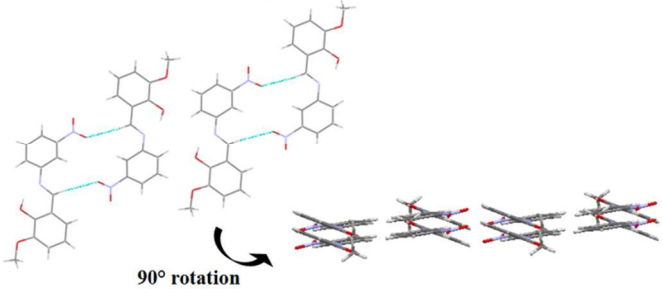


**Fig. 4** Single layer of molecules in the crystalline network of triclinic polymorph II. Green dotted lines indicate dimers stabilized by single O···H short contact interactions (distance O1-H7: 2.61(5) Å).

Simulated crystal habits (BFDH model)[12] are presented in Figure 5 and compared with experimental single crystals morphologies. The prediction of the habit based on BFDH model reproduces fairly the morphologies of the crystals under study. Geometrical parameters of hydrogen bonds for the two polymorphs are given in Table 2. In both cases, the only first-level graph-set detected is $S_1^1(6)$, meaning that an intramolecular hydrogen bond motif is formed by one dimer of hydrogen bond donor-acceptor in the same molecule.

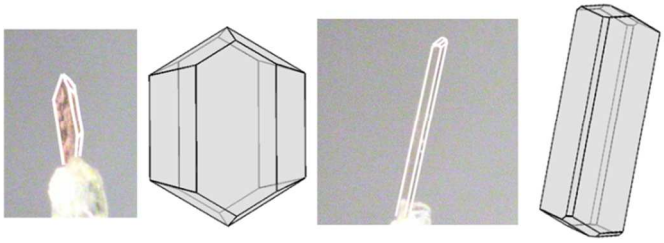

**Fig. 5** Comparison between the calculated and the experimental morphologies for polymorph I (left) and polymorph II (right).

**Table 1.** Main Crystallographic Data for Polymorphs I and II.

| | | Polymorph I | Polymorph II |
|---|---|---|---|
| **Crystal data** | Empirical formula | $C_{14}H_{12}N_2O_4$ | $C_{14}H_{12}N_2O_4$ |
| | Fw | 272.26 | 272.26 |
| | Crystal system | Orthorhombic | Monoclinic |
| | Space group | Pbca (No. 61) | ($P\bar{1}$) (n. 2) |
| | a, b, c (Å) | 12.8418(3)<br>7.5487(2)<br>26.4610(6) | 4.7895(3)<br>11.3446(10)<br>12.0610(9) |
| | α, β, γ (°) | 90 90 90 | 93.472(7) 100.357(6)<br>94.022(6) |
| | V (Å$^3$) | 2565.10(11) | 641.28(9) |
| | Z | 8 | 2 |
| | $\rho_{calcd}$ (g/cm$^3$) | 1.410 | 1.410 |
| | Mu (/mm) | 0.882 | 0.882 |
| | F(000) | 1136 | 284 |
| | Crystal size (mm) | 0.04 / 0.12 / 0.38 | 0.04 / 0.05 / 0.50 |
| | T (K) | 293(2) | 293(2) |
| **Collection data** | Radiation (Å) | Cu Kα : 1.54184 | Cu Kα : 1.54184 |
| | θ min. & max. (°) | 3.3 - 67.5 | 3.7 - 66.6 |
| | Tot., Uniq., R(int) | 6547, 2290, 0.025 | 3990, 2242, 0.022 |
| | Obs. data | 1948 | 1863 |
| **Refinement** | R[I > 2σ(I)] | 0.0398 | 0.0414 |
| | wR2[all] | 0.1172 | 0.1270 |
| | GoF | 1.05 | 1.06 |
| | Residual density | -0.15, 0.18 | -0.16, 0.12 |

**Table 2.** Geometrical Parameters for H-bonds in Polymorphs I and II.

| Implicated atoms in H-bonds | D···A distance (Å) | H···A distance (Å) | D-H···A angle (°) |
|---|---|---|---|
| *O3 -- H3O ··· N1 (Form I)* | 2.59(2) | 1.75(2) | 151(2) |
| *O3 -- H3O .. N1 (Form II)* | 2.61(2) | 1.78(2) | 152(2) |

**Table 3.** Geometrical Parameters for π-π / CH- π Interactions.

| Implicated atoms in π-π stacking (Form I) | Cg1-Cg2 distance (Å) | *da* distance (Å) | *mpd* distance (Å) |
|---|---|---|---|
| *Cg1: C1 to C6* | 3.62(9) | 1.85(1) | 3.45(3) |
| *Cg2$^i$: C8 to C13* | / | / | 3.46(2) |
| **Implicated atoms in CH-π interactions (Form I)** | **Cg2···H distance (Å)** | **Cg2 ···C distance (Å)** | **C-H···Cg2 angle (°)** |
| *C11-H1 ··· Cg2$^i$* | 2.88(1) | 3.72(4) | 151.4(2) |

*[i] = -x, -y, -z, da: dihedral angle between ring planes, mpd: mean perpendicular distance between a centroid and the opposite plane.*

Hirshfeld surfaces have been calculated in order to explore the packing mode and the intermolecular interactions of the molecules in the crystal. The histogram in Figure 6 gives the percentage contributions of each intermolecular contact type to the global Hirshfeld surfaces, for both polymorphic forms. It can be clearly seen that the percentage repartition is really

similar between the two polymorphs. In each case, the highest contribution to the surface is due to H···O interactions (33 % and 35 %, respectively).

Other significant contributions derive from H···H and H···C contacts and lower contributions are associated to C···C contacts. Although the repartitions of each type of interactions are similar, significant differences are detected by 2D-fingerprint plots analysis (Figure 7). Inspection of the 2D-fingerprint plot for polymorph I crystals reveals a peak (highlighted in red in Figure 7) in the H···H contact area. This peak is due to a contact between the hydrogen on the C6 aromatic carbon and a hydrogen atom of the methoxy group of an adjacent molecule. Another interesting difference is the wing-shape area (highlighted in yellow on Figure 7) which indicates C-H···π contacts (particularly C5-H···π), further stabilizing the packing (Figure 7). The green area on the central zone of the 2D-fingerprint plot describes significant π-π stacking interactions.

A survey on the CSD was also performed for structures similar to compound (**1**). This allowed the statistical evaluation of the values distribution for torsion angles C7-N1-C4-C3 (T1) and N1-C7-C8-C13 (T2) in related crystal structures. It also allows the rationalization of the influence of an intramolecular H-bond on the T2 torsion angle value. To gain insights about the T2 torsion angle value, two different surveys on the CSD have been performed. Firstly, a generic Schiff base has been used as query (synthon in Figure 8, top).

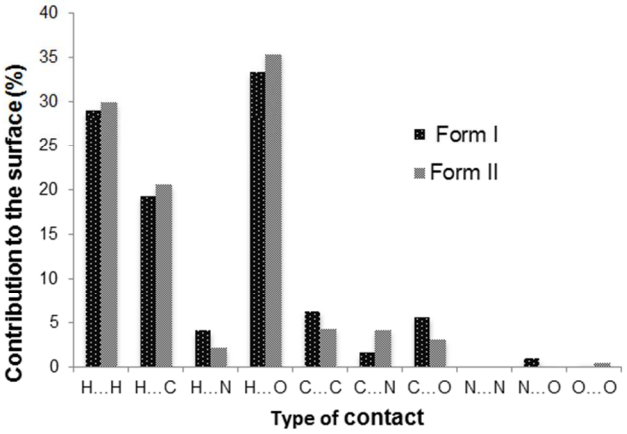


**Fig. 6** Percentage contributions of each intermolecular contact type to the global Hirshfeld surfaces (Fig. 7).

Secondly, the o-hydroxyl group has been added in the searching synthon (Figure 8, middle). In both cases, the coplanar conformation is the most stable, but in the second search, T2 values show a narrower distribution around 0°. The *ortho*-hydroxylated Schiff bases prefer to adopt the 0° conformation to allow the electronic delocalization between phenyl and imino group and intramolecular H-bond formation. Figure 8 (bottom) also presents a histogram with the statistical repartition of T1 values. Highest values are detected at 0° and 180° meaning that the coplanar conformation is the most frequent.

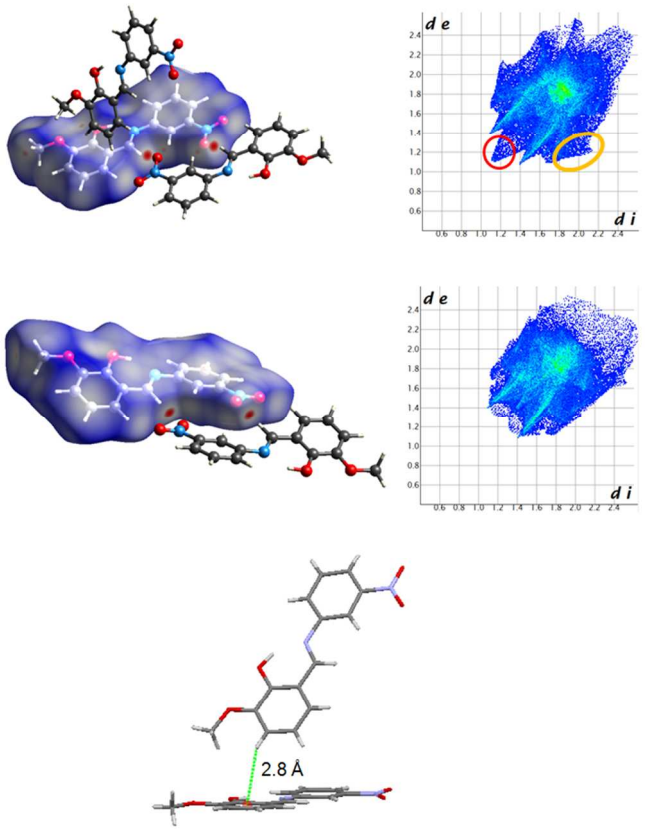


**Fig. 7** Hirshfeld surfaces ($d_{norm}$ function) and 2D molecular fingerprint plots of Hirshfeld surfaces for polymorph I (top) and polymorph II (middle) crystals, CH···π interaction in polymorph I (bottom, Table 3).

Moving away from the co-planarity, the number of structure decreases, with an exception around 30°, 150°, 210° and 330°. These observations are consistent with the experimental structures reported in this work.

The variation of conformational energy for T1 and T2 has been calculated by a DFT 1D conformational scan and compared with the frequency of occurrence of these values in the structure-like molecules reported in the CSD (Figure 8).

As might be expected, T1 rotation has only a minor effect on conformational energy with a range of variation within ±9 kJ/mol (Figure 8, bottom). Global minima are found at 30° and 330° and two local minima at about 150° and 210°, suggesting the 30° tilted conformation is the most stable. In contrast to T1, T2 has a stronger effect on the conformational energy (*i.e.* range of variation within ±70 kJ/mol), confirmed by the CSD survey, (Figure 8, middle) showing that this angle is near-planar. As a consequence, the T2 torsion angle is restricted to 0°, a value which corresponds to the conformational energy global minimum.

**Crystal Structure Prediction study on the compound**

Crystal structure predictions were performed on compound (**1**) using Polymorph Predictor module in Materials Studio v.6.0. The sole aim of this part was to check whether the CSP

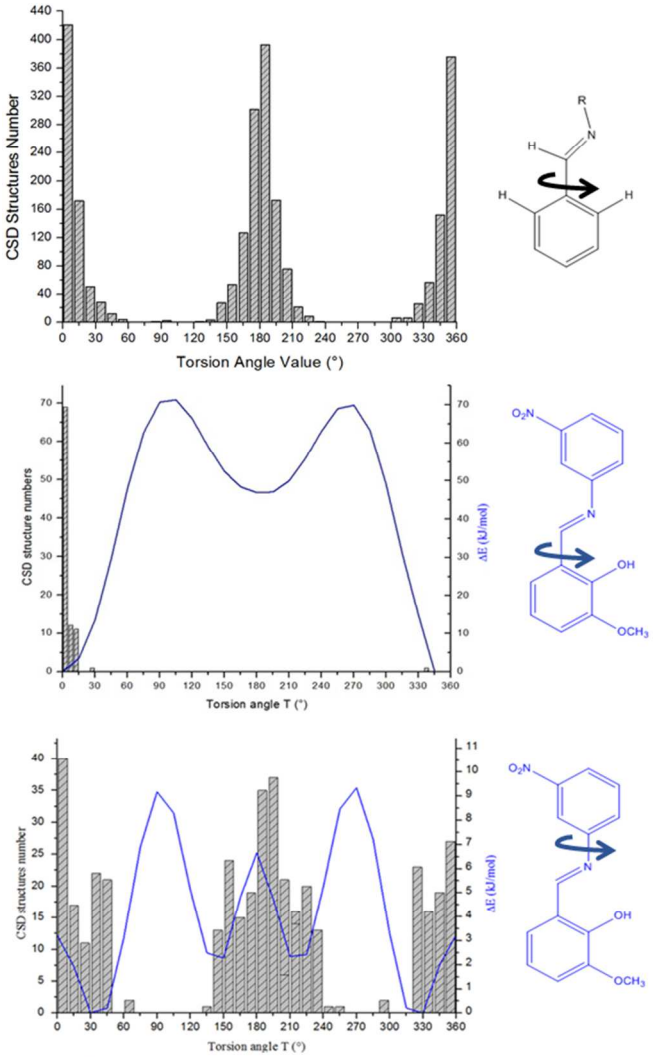


**Fig. 8** Statistical repartition of torsion angles T2 (top, middle) and T1 (bottom) in structures related to the title compound, retrieved from the CSD. Evolution of conformational energy from a conformational scan is superimposed. The synthon used for T2 CSD query (top) and the investigated torsion angle T2 (middle) and T1 (bottom) are indicated on the right side of the image, in black or blue, respectively.

approach was able to correctly predict the structures of the two conformational polymorphs and estimate their relative stability. But the goal here is not a systematic screening of all possible polymorphic forms. Therefore, only P$\bar{1}$ and Pbca space groups corresponding to both polymorphic forms were selected. Clustering of the predicted polymorphs was done using the polymorph clustering routine and is based on lattice energy and density for each crystal structure. The starting geometries for the search correspond to the two conformations of (**1**) T2 = 0 (polymorph II, Pbca) or -30° (polymorph I, P$\bar{1}$). In order to avoid relaxation of this torsion angle during the geometry optimization step (using *DMol3* approach),[13-14] T2 was fixed during the whole process (rigid group definition) to explore the conformational polymorphs. Without this, only final crystal structures corresponding to the coplanar conformation are generated, underlining the difficulty of predicting conformational polymorphs.[15]

After a final clustering step, the calculated crystal structures were ranked according to their total energy and density. The top 20 structures with low energy and high density were visually inspected to identify the packing motifs. The experimentally observed polymorphs I and II of (**1**) are predicted in the top solutions generated from both space groups (P$\bar{1}$ or Pbca) using as starting searched molecules the two conformations of (**1**) (T2=0 or -30° (rigid)) (Table 4). Predicted crystal structures close to the experimental polymorphs I and II are highlighted in Table 4 by an asterisk: [*] for polymorph I and [**] for polymorph II.

These top predicted structures generated using the Monte Carlo method[16] and minimized with the Dreiding forcefield[17] fit well to the two determined polymorphic structures as shown in Figure 9, illustrating the good agreement between the experimental structures and the predicted ones.

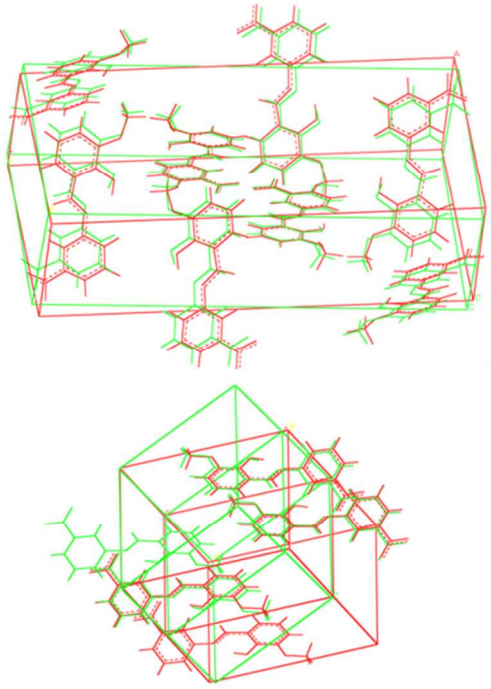

**Fig. 9** Comparison between simulated crystal structures (red) and experimental structures (green) for both polymorphs I (top) and II (bottom) of compound (**1**). The simulated crystals structures correspond to the solutions denoted [*] and [**] in Table 4.

### Calorimetric and thermochromic behaviour

The two polymorphic forms have been analysed with DSC, and exhibit close melting points (Figure 10). Form I melts at 143.5°C, whereas form II shows a melting point of 144.5°C, both without significant endothermic event before. A cooling run has also been applied for form I and II. While form I recrystallizes without any noticeable formation of form II (checked by a second heating step, $T_{cryst}$: 109.2°C), form II converted in form I after melting (Fig. S3). Thermodynamic relationship between them was assessed with the help of Burger and Ramberger rules: [18] experimental data are used to

differentiate between enantiotropic or monotropic behaviour. Table 5 summarizes experimental data carried out to determine the relationship, which in the case of forms I and II is non-ambiguously *monotropic*. In fact, there are no possibilities to switch from form I to form II before the melting point (without passing by the liquid phase). The most stable polymorph determined is the polymorph I (Pbca), with its (slightly) higher melting point. Thermodynamic behaviour is assessed by comparison between calculated $\Delta H_m$ and $\Delta S_m$ for the two forms: the polymorph with the lower melting point (form II) possesses the lower enthalpy and entropy of melting (Table 5).

In contrast to the prediction that suggests crystalline networks with different stability (Table 4), DSC shows that the relative stability of the two polymorphs must be quite similar, the close melting points providing indirect insights into the relative stability of the two crystalline networks. We can explain the differences of relative predicted stabilities by the fact that in the simulation, conformation of one of the polymorphs (T2 = -30° (rigid)) had to be fixed in order to reproduce the crystal packing. This procedure does not permit relaxation of the final structure, accounting for overestimated energies. Furthermore, the first polymorph to appear experimentally during grinding is Form II, in agreement with Ostwald's tendency rule, in which the first polymorph to appear is normally the less stable one.[19]

**Table 4.** Output of the crystal structure predictions performed on (**1**).

| Structures | Frame number | Space group | Cell (Å³, Å,°) | Density (g/cm³) | Total Energy (au) |
|---|---|---|---|---|---|
| ConfA (T2 = 0°) | 1 | $P\bar{1}$ | V = 648<br>a = 7.341<br>b = 14.807<br>c = 6.311<br>α = 101.733<br>β = 86.248<br>γ = 104.979 | 1.394 | 24.98 |
| ConfA (T2 = 0°) | 2 | $P\bar{1}$ | V = 645<br>a = 14.506<br>b = 7.339<br>c = 7.0461<br>α = 61.206<br>β = 100.664<br>γ = 97.836 | 1.402 | 25.20 |
| ConfA (T2 = 0°) [*] | 1 | Pbca | V = 2630<br>a = 7.769<br>b = 26.410<br>c = 12.822 | 1.375 | 25.49 |
| ConfA (T2 = 0°) | 2 | Pbca | V = 2630<br>a = 26.536<br>b = 12.756<br>c = 7.779 | 1.373 | 25.61 |
| rigid_ ConfB (T2 = -30°) [**] | 1 | $P\bar{1}$ | V = 633<br>a = 4.663<br>b = 12.345<br>c = 11.883<br>α = 82.875<br>β = 77.784<br>γ = 71.666 | 1.427 | 118.18 |
| rigid_ ConfB (T2 = -30°) | 2 | $P\bar{1}$ | V = 636<br>a = 4.547<br>b = 11.936<br>c = 12.00<br>α = 80.676<br>β = 81.865<br>γ = 89.381 | 1.421 | 121.08 |
| rigid_ ConfB (T2 = -30°) | 1 | Pbca | V = 2640<br>a = 6.809<br>b = 26.757<br>c = 14.471 | 1.372 | 120.75 |
| rigid_ ConfB (T2 = -30°) | 2 | Pbca | V = 2640<br>a = 11.333<br>b = 6.618<br>c = 35.178 | 1.371 | 120.86 |
| *[*] cell parameters of experimental polymorph I, [**] cell parameters of experimental polymorph II* | | | | | |

**Table 5.** Physico-Chemical Data for Polymorphs I and II.

| | Polymorph I | Polymorph II |
|---|---|---|
| **Melting point (DSC onset temperature, °C)** | 143.5 | 144.5 |
| **Heat of melting (kJ/mol)** | 29.98 | 34.34 |
| **Entropy of melting (kJ/mol.°)** | 0.2067 | 0.2352 |
| **Density calculated (from X-ray diffraction, g/cm³)** | 1.410 | 1.410 |

The two solid forms have also been exposed to liquid nitrogen (77 K), by a brief immersion of a few seconds. This brutal temperature decrease is enough to induce a change of color of the two polymorphs: both samples change from red (polymorph I) and orange (polymorph II) to light yellow (Figure 11). The thermochromic effect is qualitatively demonstrated and seems to be common to both forms. But this effect does not persist for a long time: removal of the samples from liquid nitrogen leads to rapid return to the initial coloration in a few seconds. Low-temperature diffraction data have been collected on a single crystal of polymorph I to observe the structural solid-state changes at molecular level inducing the color change (and therefore the observed thermochromic effect) (Figure S4).

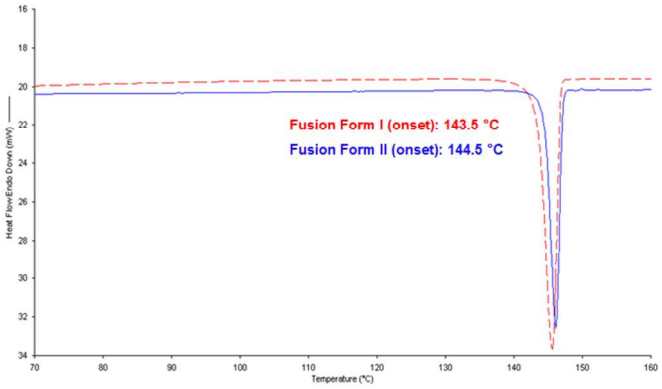


**Fig. 10** Thermograms (5K/min) for polymorphs I and II, with melting points (onset) on the diagram.

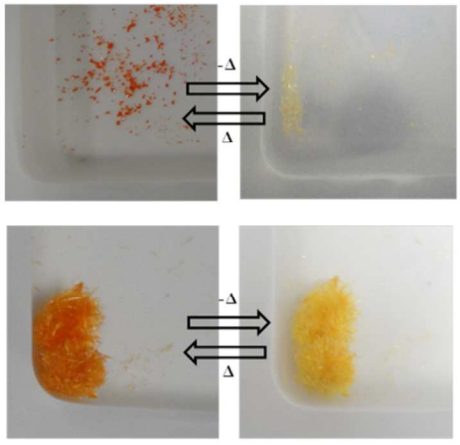


**Fig. 11** Thermochromic intrinsic behaviour of the two polymorphs I (top) and II (bottom). Orange/red coloration is observed at room temperature (left) and pale yellow coloration at 77K (right).

Placed in the nitrogen stream (105 K), the single crystal instantaneously changed from orange to pale yellow, confirming the observation made on the bulk powder. Several conclusions can be drawn from the low-temperature structural results: firstly, the expected form was the *keto* tautomer, *enol-keto* tautomerism being claimed in the case of anil derivatives to be essential for the thermochromic behaviour.[2-5,20] The low temperature crystal structure we obtained mainly corresponds to the enol tautomer, like in our room temperature structure. Fourier difference maps show a weak residual electronic density peak located near the N1 nitrogen atom (at a distance of 0.88 Å), compatible with a slight *keto* character for the low-temperature structure. Furthermore, distance between N1 nitrogen atom and C7 carbon atom is significantly longer at low temperature (1.284(2)) than the normally double bond in a pure *enol* form, (bond length in the room temperature structure : 1.279(1) Å). Both elements suggest a slight *keto* character in the crystal structure obtained at low temperature. An average structure has been refined with low-temperature data (Figure S4). These experimental observations are in good agreement with literature structural data on similar derivatives.[20] Indeed, attempts to observe the *keto* (or zwitterionic) form by crystal data collected at low temperature have been unsuccessful unless the presence in the structure of an intermolecular hydrogen bond implying the hydroxyl moiety and stabilizing the *keto*/zwitterionic form. In the case of compound (**1**), assessment by crystallography of the tautomer conversion at low-temperature from *enol* form to *keto* form seems to be questionable, as we end up with a structure that mainly corresponds to a mixture of the *enol* tautomer (major component) and some (minor) contribution from the *keto* form.

## Experimental

*Materials: ortho*-vanillin (*2-hydroxy-3-methoxybenzaldehyde*) and 3-nitroaniline were sourced from Sigma-Aldrich (Steinheim, germany) (>99% chemical purity) and used as received. Solvents used for crystallization (EtOH, MeOH and toluene from Acros Organic, Geel, Belgium) are commercially available and were used without further purification.

*Mechanosynthesis:* Dry grinding was performed by means of a Retsch Mixer Mill 400 (50' / 30 Hz), equipped with two grinding jars in which five 2-mL Eppendorf tubes can be installed with eight to ten stainless steel grinding balls (1 mm diameter) in a sample. Each sample before grinding contains 1 mmol of *ortho*-vanillin (152 mg) and 1 mmol of 3-nitroaniline (138 mg).

*Single X-ray diffraction (SCXRD):* SCXRD experiments were performed on an *Oxford Diffraction Gemini R. Ultra diffractometer* (4-circle kappa platform, Ruby CCD detector) using a Cu Kα (λ = 1.54184 Å) radiation for the two polymorphs at room temperature and with a Mo Kα (λ = 0.71073 Å) radiation for the low temperature measurement. Data reduction and cell refinement were carried out using CrysAlisPro. Structures were solved with the WinGX Suite of programs using Sir-97[20] and refined with SHELXL-97[21]. Non-hydrogen atoms were anisotropically refined, and the hydrogen atoms (not present in H-bonds) were fixed in the riding mode with isotropic temperature factors fixed at 1.2 times U(eq) of the parent atoms (1.5 times for methyl groups). Hydrogen atoms implicated in hydrogen bonds were localized by Fourier difference maps (ΔF).
For low-temperature experiment, determination of the potential hydrogen on the nitrogen N1 was also localized by Fourier difference maps (ΔF). Structures have been deposited in the CCDC databank (entries 1044084 for polymorph I, 1044161 for polymorph II and 1052602 for low-temperature polymorph I) and can be obtained free of charge via www.ccdc.cam.ac.uk/conts/retrieving.html (or from the Cambridge Crystallographic Data Center, 12, Union Road, Cambridge CB21EZ, UK; fax: +44−1223−336033; or deposit@ccdc.cam.ac.uk. Details of data collection and structure refinement are listed in Table 1, geometrical parameters for hydrogen bonds are presented in Table 2 and geometrical parameters for π-π and CH-π interactions are listed in Table 3. For the two polymorphs studied here (and the low-temperature structure), three CIF files are provided as Supporting Information.

*Structure visualization and exploration of the crystal packing:* Images from structural data were drawn with Mercury v. 3.1.[22]

*Rationalization of the intermolecular interactions:* Hirshfeld surfaces mapped with $d_{norm}$ function and 2D molecular fingerprint plots were used in order to rationalize intermolecular interactions. The calculated surfaces are mapped using the Auto function of color scaling of Crystal Explorer v. 3.1.[23]

*Crystal habit prediction:* Simulated morphology has been calculated starting from the crystallographic data with Mercury v. 3.1,[22] using the BFDH method.[12]

*Differential Scanning Calorimetry (DSC):* DSC experiments were performed from 30°C to 165°C at the scanning rate of 5°C/min on a Perkin Elmer DSC 7.0, equipped with the data analyzer program PYRIS 1997-1998. The melting peaks were integrated with a linear baseline. Calibration was made with indium (mp: 156.6 8C) standard. A mass of about 3 mg was placed in pierced aluminum sample pans with sealed lids to be analyzed and an empty aluminum pan was used as reference. Nitrogen was used as purge gas in order to prevent condensation in the cells. All DSC analyses were carried out in duplicate.

*Search in the Cambridge Structure Database (CSD):* A statistical survey on the CSD (version 5.36, last updated November 2014) was performed on compound (**1**) like-structures (with three two-dimensional representations depicted in Figure 8 as search groups) to statistically evaluate the values associated to torsion angles C7-N1-C4-C3 (T1) and N1-C7-C8-C13 (T2) and to rationalize how the presence of intramolecular H-bond affects the T2 torsion angle value. No other restrictions (such as R-factor or disorder) were applied during the search.

*Conformational Torsion Angle Analysis by Quantum Mechanics Calculations:* The energy barrier associated with the rotation of the two aforementioned torsion angles T1 and T2 was calculated through a 1D relaxed conformational scan (from 0.0 to 360 degrees by 15.0 degrees increments). Calculation have been performed with Gaussian09 on PBE1PBE/6-311G(d,p) level of theory.[24] Convergence was assumed when the r.m.s. force was smaller than $3.10^{-4}$ au and the SCF convergence criterion was set to $10^{-8}$ au.

*Crystal structure prediction (CSP):* For all solid-state simulations, the Ewald method was used for the electrostatic and van der Waals interaction terms. Electrostatic potential derived charges were used for calculations. Conformations of title compound (**1**) corresponding to the two polymorphic forms (I and II) were taken from the corresponding crystal structures obtained in the present work. These crystal structure conformations correspond to low energy conformation as deduced from the *ab initio* calculations and were used as the starting points for crystal structure prediction using the Materials Studio Polymorph Predictor. Prior to the CSP procedure, both starting geometries were optimized (Dmol3 v.6,[13-14] basis: dnp, functional: PBE,[25] scf_density_convergence: $10^{-5}$, scf_charge_mixing: 0.2000, scf_iterations: 50). The procedure includes 4 steps (Packing, Clustering, Geometry Optimization, and Final Clustering) and default settings were used. In particular, the simulated annealing algorithm (packing) used a maximum number of 7000 steps, a temperature range of 300-100000.0 K with a heating factor of 0.025 and required 12 consecutive steps to be accepted before cooling. The Dreiding force field was used for energy calculation. Ewald summation (accuracy: 0.0001 kcal/mol) was used for the electrostatic and van der Waals terms while the atom-base summation method (truncation method: cubic spline, 4.5 Å cutoff distance, 0.5 Å spline width) was used for the hydrogen bond terms. Convergence tolerances for geometry optimizations are 0.0001 kcal/mol for the energy, 0.005 kcal/mol/Å for the force, and $5.10^{-5}$ Å for displacement. CSP calculations were performed for both $P\bar{1}$ and Pbca space groups corresponding to both polymorphic forms. Clustering of the predicted polymorphs was done using the polymorph clustering routine in Materials Studio and is based on lattice energy and density for each crystal structure.

## Conclusions

Our present work focuses on an in-depth structural characterization, combining X-ray crystallography and computational methods, of *(E)-2-methoxy-6-{[(3-nitrophenyl)imino]methyl}phenol*. The compound could quantitatively be synthetized by mechanochemical synthesis using ball milling and grinding starting from the corresponding 3-nitro aniline and *ortho*-vanillin. Crystallization was performed by slow evaporation and two different crystalline forms, I and II, have been obtained. To the best of our knowledge, this compound is one of the first cases of proved polymorphism for N-salicylidene aniline derivatives so far.

A DFT 1D conformation scan has been performed on T1 and T2 torsion angles to gain insight about the overall shape of the molecule. The calculated conformations substantially reflect the experimental ones deduced from SCXRD crystallography. T2 has been found to have a strong effect on the conformational energy of the compound. The computational results have been corroborated by a statistical study of T1 and T2 values on data in the CSD.

Crystal structure predictions were able to produce, a posteriori, the two conformational polymorphs. In this simulation, it was absolutely necessary to fix the conformation of the molecule to be able to generate the polymorph corresponding to the less stable conformation. In this case, extra structural data had to be included in the simulation to be able to predict structures in good agreement with the experimental structures of polymorphs I and II of (**1**). This introduces a bias in the estimation of the relative energies between the two polymorphs as deduced by DSC measurements that show the two polymorphs having similar melting points, in contrast to what would be expected from the simulations. Both polymorphic forms show similar thermochromic behaviour in the solid state, and work is in progress to better understand the structural changes inducing this intrinsic characteristics. Potential photochromic behaviour (in solution and also at solid-state) will be thoroughly investigated, and thermodynamic relationship between the two polymorphic forms will also be assessed and described.

Starting from nothing, the difficulty to correctly predict potential conformational polymorphism for a single molecule has been highlighted again, especially if no experimental data can support the process. This example proves once more that computational effort has really to be accomplished at academic level in view of better '*ab initio*' structural solid-state prediction.

## Acknowledgements

Authors are grateful to Ms Bernadette Norberg for the data collection and for her continuous interest on this work. This research used resources of the 'Plateforme Technologique de Calcul Intensif' (http://www.ptci.unamur.be) which is supported by the F.R.S.-FNRS and is member of the 'Consortium des Équipements de Calcul Intensif' (http://www.cecihpc.be).

## Notes and references

† Final product obtained by grinding: $^1$H NMR (400 MHz, $CDCl_3$, 298 K): δ = 8.71 (s, 1H), 7.31 (d, J = 8.24 Hz, 3H), 7.23 (d, J = 8.24 Hz, 2H), 7.01 (dd, $^1$J = 8.01 Hz, $^2$J = 1.37 Hz, 1H), 6.91 (t, J = 7.90 Hz, 1H) 3.94 ppm (s, 3H). Chemical shifts were reported in ppm according to tetramethylsilane, using the solvent residual signal as an internal reference.

[a] *Unité de Chimie Physique, Théorique et Structurale, Chemistry Department, 61 rue de Bruxelles, B-5000 Namur,University of Namur, Belgium. Tel: +32 (0)81/72.45.50*
* *Email: johan.wouters@unamur.be*

Electronic Supplementary Information (ESI) available: .Cif datafiles from SCXRD for the two polymorphic structures are included in ESI. See DOI:

1 H. I. Bernstein, W. C. Quimby, *J. Am. Chem. Soc.*, 1943, **65** (10), 1845; Bernstein, J. *Polymorphism in Molecular Crystals* (Vol. 14), 2007, Oxford University Press; J. Bernstein , A. T. Hagler, *J. Am. Chem. Soc.*, 1978, **100** (3), 673; S. P. Delaney, T.M. Smith, T.M. Korter, *J. Mol. Struct.*, 2014, **1078**, 83; S. S. Kumar, A. Nangia, *CrystEngComm*, 2013, **15**(33), 6498; E. Babjakova, B. Hanulikova, L. Dastychova, I. Kuritka, M. Necas, R. Vicha, *J. Mol. Struct.*, 2014, **1078**, 106; S. M. Pratik, A. Nijamudheen, S. Bhattacharya, A. Datta, *Chem. Eur. J.*, 2014, **20**(11), 3218, J. R. Smith, W. Xu, D. Raftery, *J. Phys. Chem. B.*, 2006, **110**(15), 7766.
2 E. Hadjoudis, I.M. Mavridis, *Chem. Soc. Rev.*, 2004, **33**, 579.
3 F. Robert, A.D. Naik, B. Tinant, R. Robiette and Y. Garcia, *Chem. Eur. J.*, 2009, **15**, 4327.
4 F. Robert, A.D. Naik, F. Hidara, B. Tinant, R. Robiette, J. Wouters and Y. Garcia, *Eur. J. Org. Chem.*, 2010, 621.
5 F. Robert, P.L. Jacquemin, B. Tinant, and Y. Garcia, *CrystEngComm*, 2012, **14**, 4396.
6 K. Johmoto, A. Sekine and H. Uekusa, *Cryst. Growth Des.*, 2012, **12**, 4779.
7 J. Cusido, E. Deniz and F.M. Raymo, *Eur. J. Org. Chem.*, 2009, 2031.
8 J. Zhang, Q. Zou and H. Tian, *Adv. Mater.*, 2013, **25**, 378.
9 T. Kim, L. Zhu, R.O. Al-Kaysi and C.J. Bardeen, *ChemPhysChem*, 2014, **15**, 400.
10 K.M. Hutchins, S. Dutta, B.P. Loren and L.R. MacGillivray, *Chem. Mater.*, 2014, **26**, 3042.
11 M. Zbacnic and B. Kaitner, *CrystEngComm*, 2014, **16**, 4162.
12 J. D. H. Donnay and D. Harker, *Am. Mineral.*, 1937, **22**, 446.
13 B. Delley, *J. Chem. Phys.*, 1990, **92**, 508.
14 B. Delley, *J. Chem. Phys.*, 2000, **113**, 7756.
15 H. D. Clarke, K. K. Arora, H. Bass, P. Kavuru, T. T. Ong, T. Pujari, L. Wojtas and M. J. Zaworotko, *Cryst. Growth Des.*, 2010, **10**, 2152.
16 C.Jacoboni and L. Reggiani, *Rev. Mod. Phys.*, 1983, **55**, 645.
17 S.L. Mayo, B.D. Olafson and W.A. Goddard, *J. Phys. Chem.*, 1990, **94**, 8897.
18 M. J. Buerger, *Crystallographic aspects of phase transformations.* In R. Smoluchowski, J.E. Mayer, W.A. Weyl, (Eds.), *Phase Transformations in Solids*, John Wiley and Sons, New York, 1951, 183 ; A. Burger, R. Ramberger, , *Mikrochim. Acta*, 1979, 259, A. Grunenberg, J.-O. Henck,

H.W. Siesler, *Int. J. Pharm.*, 1996 **129**, 147; A. Burger, R. Ramberger, *Mikrochim. Acta*, 1979, 273; A. Burger, *Acta Pharm. Technol.*, 1982, **28**, 1.

19 W. Ostwald, *Zeitschrift für Physikalische Chemie*, 1897, **22**, 289 ; T. Threlfall, *Org. Process Res. Dev.*, 2003, **7**(6), 1017.

20 K. Ogawa, Y. Kasahara, Y. Ohatni, J. Harada, *J. Am. Chem. Soc.* 1998, **120**, 7107 ; T. Fujiwara, J. Harada, K. Ogawa, *J. Phys. Chem. A*, 2009, **113**(9), 1822.

21 A. Altomare, M. C. Burla, M. Camalli, G. L. Cascarano, C. Giacovazzo, A. Guagliardi, A. G. G. Moliterni, G. Polidori and R. Spagna, *J. Appl. Cryst.*, 1999, **32**, 115.

22 G. M. Sheldrick, *Acta Crystallogr., Sect. A: Cryst. Phys., Diffr., Theor. Gen. Crystallogr.*, 2008, **64**, 112.

23 Macrae, C. F.; Bruno, I. J. ; Chisholm, J. A.; Edgington, P. R.; McCabe, P.; Pidcock, E.; Rodriguez-Monge, L. ; Taylor, R.; van de Streek, J. and Wood, P. A.; J. Appl. Cryst., 2008, **41**, 466-470

24 M. A. Spackman and J. J. McKinnon, *CrystEngComm*, 2002, **4** (66), 378.

25 Gaussian 09, Revision D.01, M. J. Frisch, G. W. Trucks, H. B. Schlegel, G. E. Scuseria, M. A. Robb, J. R. Cheeseman, G. Scalmani, V. Barone, B. Mennucci, G. A. Petersson, H. Nakatsuji, M. Caricato, X. Li, H. P. Hratchian, A. F. Izmaylov, J. Bloino, G. Zheng, J. L. Sonnenberg, M. Hada, M. Ehara, K. Toyota, R. Fukuda, J. Hasegawa, M. Ishida, T. Nakajima, Y. Honda, O. Kitao, H. Nakai, T. Vreven, J. A. Montgomery, Jr., J. E. Peralta, F. Ogliaro, M. Bearpark, J. J. Heyd, E. Brothers, K. N. Kudin, V. N. Staroverov, R. Kobayashi, J. Normand, K. Raghavachari, A. Rendell, J. C. Burant, S. S. Iyengar, J. Tomasi, M. Cossi, N. Rega, J. M. Millam, M. Klene, J. E. Knox, J. B. Cross, V. Bakken, C. Adamo, J. Jaramillo, R. Gomperts, R. E. Stratmann, O. Yazyev, A. J. Austin, R. Cammi, C. Pomelli, J. W. Ochterski, R. L. Martin, K. Morokuma, V. G. Zakrzewski, G. A. Voth, P. Salvador, J. J. Dannenberg, S. Dapprich, A. D. Daniels, Ö. Farkas, J. B. Foresman, J. V. Ortiz, J. Cioslowski, and D. J. Fox, Gaussian, Inc., Wallingford CT, 2009.

26 J.P. Perdew, K. Burke and M. Ernzerhof, *Phys. Rev. Lett.*, 1996, **77**, 3865.



 

Solid-state polymorphism behaviour of a new thermochromic mechanosynthesized compound derived from ortho-vanillin is investigated through SCXRD and *ab initio* prediction methods.